ACS central science

http://pubs.acs.org/journal/acscii

Research Article

# h-FIBER: Microfluidic Topographical Hollow Fiber for Studies of Glomerular Filtration Barrier

Ruoxiao Xie, Anastasia Korolj, Chuan Liu, Xin Song, Rick Xing Ze Lu, Boyang Zhang, Arun Ramachandran, Qionglin Liang,* and Milica Radisic*

Cite This: https://dx.doi.org/10.1021/acscentsci.9b01097

Read Online

ACCESS | Metrics & More | Article Recommendations | Supporting Information

**ABSTRACT:** Kidney-on-a-chip devices may revolutionize the discovery of new therapies. However, fabricating a 3D glomerulus remains a challenge, due to a requirement for a microscale soft material with complex topography to support cell culture in a native configuration. Here, we describe the use of microfluidic spinning to recapitulate complex concave and convex topographies over multiple length scales, required for biofabrication of a biomimetic 3D glomerulus. We produced a microfluidic extruded topographic hollow fiber (h-FIBER), consisting of a vessel-like perfusable tubular channel for endothelial cell cultivation, and a glomerulus-like knot with microconvex topography on its surface for podocyte cultivation. Meter long h-FIBERs were produced in microfluidics within minutes, followed by chemically induced inflation for generation of topographical cues on the 3D scaffold surface. The h-FIBERs were assembled into a hot-embossed plastic 96-well plate. Long-term perfusion, podocyte barrier formation, endothelialization, and permeability tests were easily performed by a standard pipetting technique on the platform. Following long-term culture (1 month), a functional filtration barrier, measured by the transfer of albumin from the blood vessel side to the ultrafiltrate side, suggested the establishment of an engineered glomerulus.

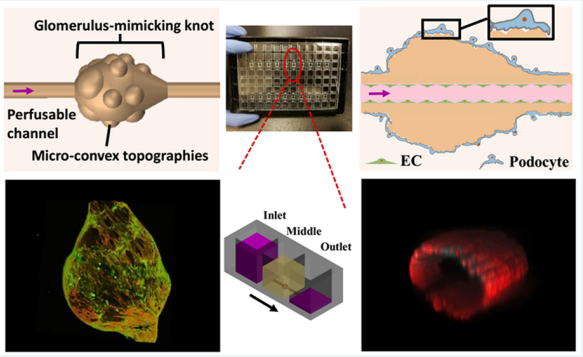


## 1. INTRODUCTION

Organ-on-a-chip devices are poised to revolutionize pathophysiological studies and drug discovery. Specifically, kidney-on-a-chip devices are of particular interest, since the incidence of diabetic and hypertensive nephropathy is on the rise as the population continues to age, and nephrotoxicity is also one of the key reasons for the withdrawal of already approved drugs.[1−3] The kidney is an incredibly complex organ, consisting of 26 different cell types in a precise geometrical and structural arrangement.[4] It is the precise structure and orientation of these cells that are responsible for the remarkable filtration function of the kidney.

Most kidney diseases have been recognized to begin with the dysfunction of the glomerulus.[5,6] The glomerulus functions as the major filtration unit of the kidney, where plasma is filtered to form concentrated urine. Considerable efforts have, therefore, been made to build an *in vitro* glomerulus model to better understand this filtration unit.

Developed from the self-organization of pluripotent or adult stem cells, kidney organoids have offered a notable approach for the modeling of kidney development and diseases *in vitro*.[7−9] While cells with the characteristics of glomerular podocytes and glomerulus-like compartments were present in these organoids, vascular flow and functional tests through the *in vitro* kidney organoids were never realized due to their immaturity.[10,11] Though early glomerulus models, which made use of a transwell device where cells were cultured on the porous membrane, allow functional tests of cell barrier function, these static models can hardly recapitulate the flow environment of the glomerulus.[12,13] Recently, advances in microfluidics have made it possible to further mimic the biomechanical microenvironment *in vitro*.[14,15] Flow or dynamic mechanical strain, focused on reproducing aspects of the glomerular environment, was exerted onto the glomerulus-derived cells, which have been cultured on a membrane within the microfluidic chip.[16−18] The fluid was demonstrated to enhance the survival of isolated glomerular microtissues and the modeling of physio-pathological fluid environments to enable more biomimetic glomerulus models.[19,20] By combining strain with physiological flow, Musah et al. demonstrated that the differentiation of human induced pluripotent stem cells into podocytes was enhanced, enabling the fabrication of a human glomerulus-on-a-chip model.[21]

Received: October 27, 2019

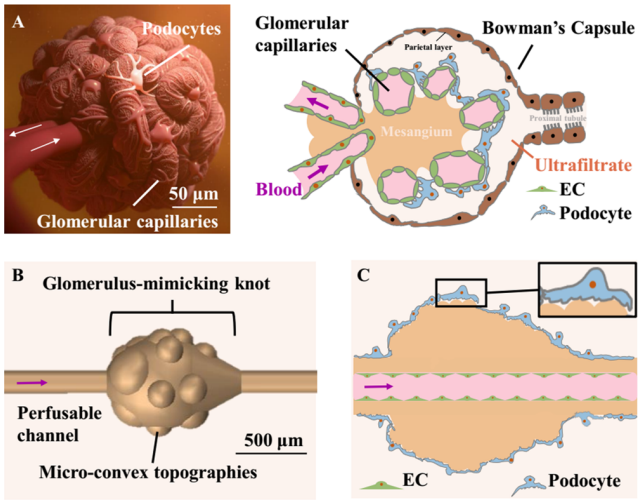


**Figure 1.** Design of the biologically inspired h-FIBER. (A) Glomerulus structure. (B) 3D structure of the h-FIBER. (C) Perfusable glomerulus model based on h-FIBER. A scale bar in part A shows the size of a typical adult kidney glomerulus.[59] A scale bar in part B shows the size of a typical knot. The knot is about 3−4 times bigger than a typical glomerulus.

However, even in these advanced models, cells are still cultured in a simplified 2D geometry without recapitulating the structure of a 3D glomerulus.

The kidney glomerulus is a knot of capillaries with endothelial cells (ECs) lying inside the lumen at the blood vessel side and podocytes covering the external surface at the ultrafiltrate side (Figure 1A).[22,23] To enhance the function of *in vitro* models, appropriate structures with the intricate architecture and complexity of native organs are required.[24−27] Significant efforts have been invested in the fabrication of tubular structures to mimic blood vessels by various engineering methods.[28,29] It was demonstrated that 3D tubular structures could enable physiological force-driven endothelial behaviors, while a flat and stiff substrate would influence cell−cell signaling pathways related with the barrier function.[30−32] However, despite the feasibility of constructing various tubular scaffolds, the absence of a microscale soft material with complex topography, to enable cell coculture in a native configuration, has limited the progress toward a biomimetic 3D glomerular structure.

Here, we describe the use of microfluidic spinning to recapitulate complex concave and convex topographies over multiple length scales, required for biofabrication of a biomimetic 3D glomerulus. The technique combines high-throughput production, as meter long hollow microfibers can be generated within minutes, with chemically induced inflation

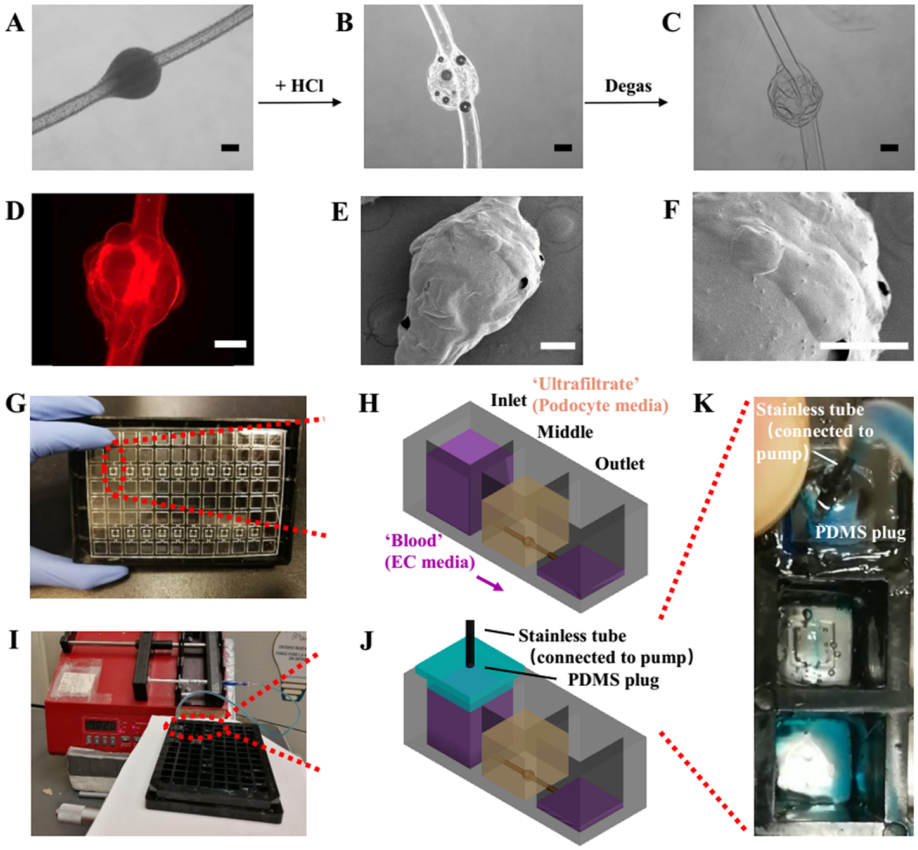


**Figure 2.** Fabrication of glomerulus-on-a-plate platform. (A−C) The generation of the microconvex topography on the hydrogel knot surface using chemically induced inflation method. (A) Knotted hydrogel microfiber with embedded $CaCO_3$ beads. (D) Fluorescent image of the h-FIBER (TRITC-conjugated fluorescent beads were embedded in the hydrogel). (E) Low-magnification and (F) high-magnification SEM image showing the microconvex topography on the scaffold surface. (G) Assembly of the h-FIBERs into a 96-well plate. (H) Gravity-driven perfusion of the h-FIBER. (I) Perfusion of the h-FIBER by the syringe pump. (J) Schematics of the syringe pump connection. (K) Pump-driven flow at 70 $\mu$L/min (blue food dye indicator). Scale bars: 200 $\mu$m.


https://dx.doi.org/10.1021/acscentsci.9b01097
ACS Cent. Sci. XXXX, XXX, XXX−XXX

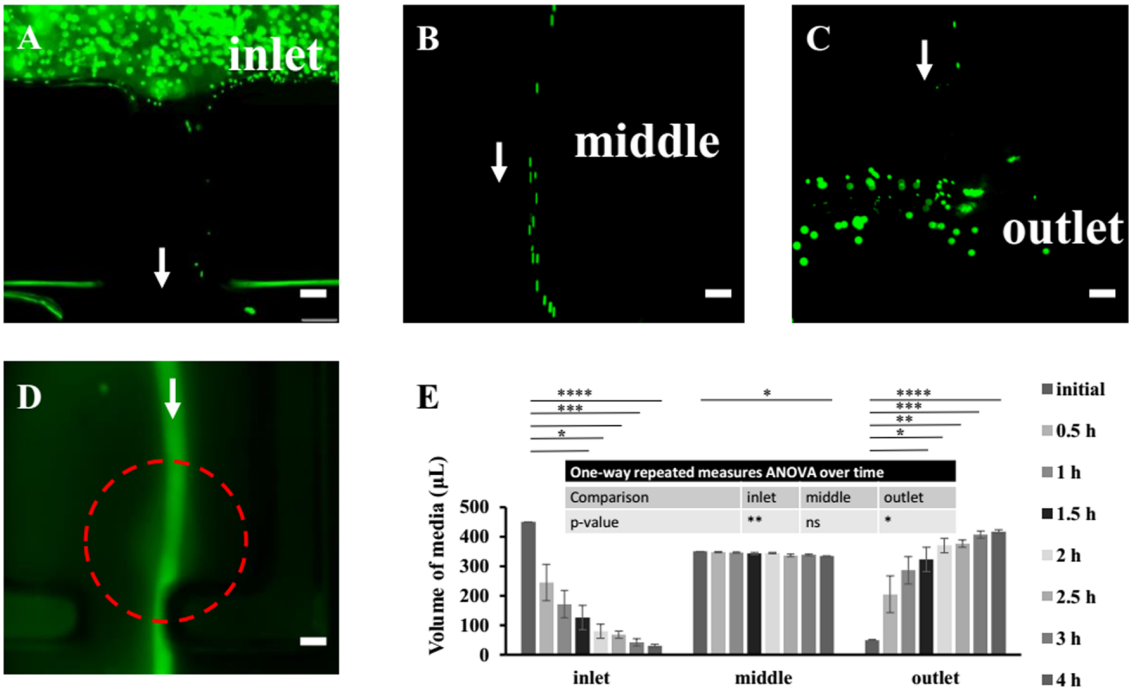


**Figure 3.** Assembled h-FIBERS are perfusable. (A−C) Fluorescence images of the inlet, middle, and outlet wells perfused with the fluorescent beads. The arrow shows the direction of the flow. (D) Fluorescence image showing the perfusion and permeation of FITC-BSA. The arrow shows the direction of the flow. The dotted line shows the location of the glomerulus-mimicking knot. (E) Quantitative results of perfusion. The *p*-value of one-way repeated measures ANOVA over time for volume of media in inlet, middle, and outlet well is 0.0087 (**), 0.0694 (n.s.), and 0.0113 (*) respectively. Data are shown as average ± s.d., $n = 3$. * $p < 0.05$, ** $p < 0.01$, *** $p < 0.001$, **** $p < 0.0001$. Scale bars: 200 $\mu$m.

of the hydrogel for instantaneous production of microscale topographical cues on the 3D microfiber surface. We term this scaffold h-FIBER, consisting of a perfusable circular channel to mimic the vascular lumen, a spindle knot to model the globular architecture of a whole glomerulus, and microconvex topography on the knot surface to recapitulate the varying patterns of capillary loops (Figure 1B,C). Different from flat 2D membranes for endothelial cell/podocyte coculture, our 3D biomimetic glomerulus is situated in a custom-made hot-embossed 96-well plate fabricated from tissue culture polystyrene to enable cell seeding, maintenance, and perfusion via gravity-driven flow, requiring no external pumps and allowing for facile liquid handling. Enhanced podocyte interdigitation was demonstrated on the knot regions of h-FIBER, compared to the tube regions. Interdigitation was further enhanced to support appropriate barrier function when these knot regions were decorated with microtopography. With the EC layer in the circular lumen, a functional glomerulus-on-a-plate platform was established, demonstrating a potential use in bioengineering and biomedical applications.

## 2. RESULTS AND DISCUSSION

The h-FIBERs were first generated from a coaxial microfluidic device by hydrogel polymerization (Figure S1).[33] Hollow microfibers with 10 knots can be fabricated within 1 min, which were then cut and used to build 10 glomerulus models in the custom designed 96-well plates. A novel chemically induced inflation method was developed to generate microconvex topography on the hydrogel surface (Figure 2A−C, Figure S2). Similar to how we blow soap bubbles by expanding air inside a soap solution, microconvex topography on the h-FIBER was created by a simple chemical reaction between $CaCO_3$ and $H^+$, to generate $CO_2$ gas. These gas bubbles were trapped, expanding the hydrogel and leaving convex structures on the hydrogel surface (Figure 2D−F). The generated knot sizes were 650−950 $\mu$m (Figure S3).

To facilitate cell attachment, RGD-conjugated alginate was used for all experiments. The diffusivity of various molecules in alginate has been reported to be high (Table S1),[34−38] suggesting its feasibility for constructing a glomerulus model. By assembling and sealing the base, together with the scaffolds, onto a bottomless custom-made 96-well plate, the h-FIBERs were then fixed inside the plate with the knot in the chamber of the middle well and the two ends in the inlet and outlet wells (Figure 2G). Up to 20 h-FIBERs were assembled into one plate at the same time. Gravity-driven perfusion was realized in these scaffolds by applying the hydrostatic pressure difference between inlet and outlet (Figures 2H and 3A−C, Video S1).[39−41] By connecting the plate to a syringe pump, fluid could also be pumped in the channel without leaking (Figure 2I−K). The perfusion of FITC-conjugated bovine serum albumin (FITC-BSA) solution in the lumen (Figure 3D) further demonstrated that the perfused media remained in the lumen, flowing from the inlet to the outlet (Figure 3E), while molecules (e.g., BSA) from the media could permeate the hydrogel and diffuse into the middle well. By reversibly tilting the plate every 3 h, long-term perfusion was easily realized. The calculated shear stress induced by the gravity-driven flow in the lumen ranges from 0.3 to 0.9 Pa, which is within the physiological range of blood flow-induced shear stress in a glomerulus (about 0.1−9.5 Pa).[42]

To fabricate the glomerulus model, a podocyte barrier should be established on the external surface of the glomerulus-mimicking h-FIBER. As cells tended to slip to the bottom rather than settle down on the microscaffold during seeding (Figure S4A−C), we developed a hanging-droplet cell


https://dx.doi.org/10.1021/acscentsci.9b01097
ACS Cent. Sci. XXXX, XXX, XXX−XXX

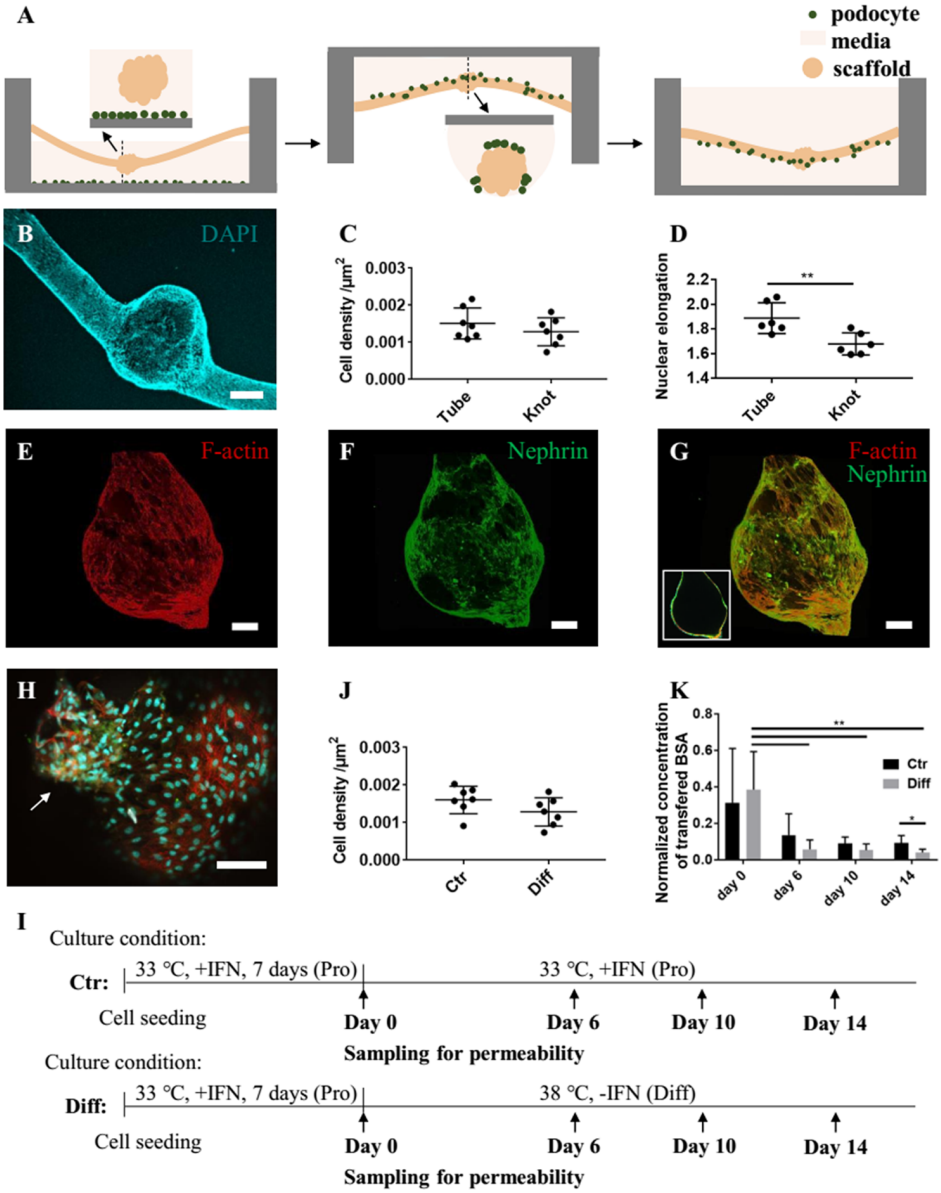


**Figure 4.** Podocytes envelop the h-FIBER forming a barrier layer. (A) Hanging-droplet cell seeding technique. (B) DAPI nuclear staining. (C) Cell density on the tube and knot. (D) Nuclear elongation on the tube and knot. (E–G) Confocal microscopy images showing the differentiated podocytes. (E) F-actin and (F) nephrin staining. (G) The merged image of F-actin and nephrin staining (the inset shows a longitudinal cross-section). (H) High-magnification image showing the merged image of F-actin, nephrin, and DAPI staining. The arrow points to the cells expressing more nephrin. (I) Timeline of cell culture for control and differentiation groups. (J) Cell density for the two groups at Day 14. (K) The transferred albumin concentration was measured at Day 0, Day 6, Day 10, and Day 14. The concentrations in the middle well were normalized to the concentration of transferred albumin measured for the cell-free h-FIBER on day 0. The *p*-value of one-way repeated measures ANOVA over time for the "Ctr" and "Diff" group is 0.1608 (n.s.) and 0.0015 (**), respectively. Data are shown as average ± s.d., $n = 6$. * $p < 0.05$, ** $p < 0.01$. Scale bar in part B is 200 $\mu$m. The other scale bars are 100 $\mu$m.

seeding technique to improve cell attachment on the scaffold (Figure 4A, Figure S4D–F). To maintain the integrity of h-FIBERs, $CaCl_2$ was added to the culture media in a concentration that did not affect cell viability (Figure S5). In proliferation media, the attached podocytes gradually covered the majority of the h-FIBER surface. Upon additional cultivation under differentiation conditions for 2 weeks, nuclear staining (Figure 4B) demonstrated that podocytes covered almost the entire external surface of the scaffold. The surface area of the knot is about 1 899 072 $\mu m^2$, which is about 28% of the total surface area. Interestingly, though cell density on the tube and knot showed no significant difference (Figure 4C), the cell nuclei on the knot region were less elongated than on the tube region (Figure 4D).

*In vivo*, podocyte slit diaphragms maintain glomerular filtration function. Nephrin and podocin are podocyte-specific proteins and vital components of the slit diaphragm.[43,44] Nephrin and podocin expression were confirmed in the podocyte layer formed on our scaffold (Figure 4F–H, Figure S6). Probably due to the artifacts coming from the staining and imaging processes, the staining is inhomogeneous across the different knot regions. During the staining process, part of the cell layer will touch the base of the container and thus be less exposed to the antibodies. The possible inhomogeneous


https://dx.doi.org/10.1021/acscentsci.9b01097
ACS Cent. Sci. XXXX, XXX, XXX–XXX

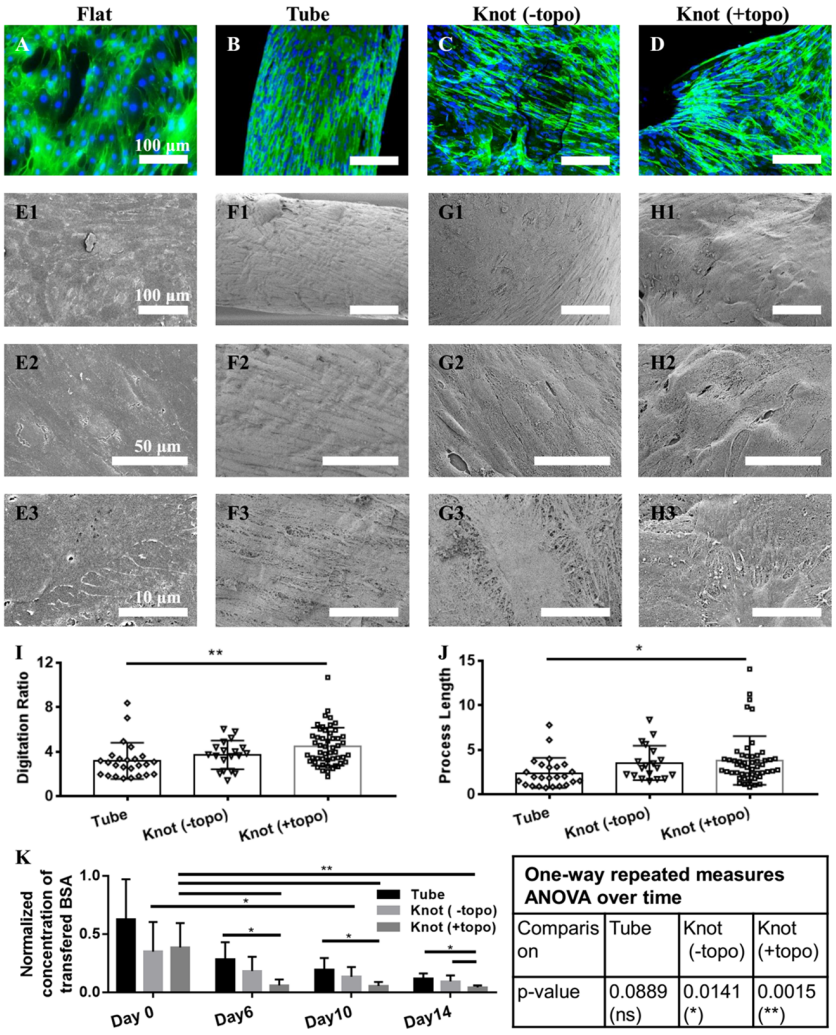


**Figure 5.** The topographical microenvironment guides podocytes' morphology and function. Merged images of F-actin and DAPI nuclear staining (A–D) and SEM images showing the cell morphology (E–H) of podocytes, cultured on the flat PDMS (Flat), hydrogel tube (Tube), hydrogel knot without microconvex topography (Knot (-topo)), and hydrogel knot with microconvex topography (Knot (+topo)), respectively. Quantification of digitation ratio (I) and process length of podocytes (J). Digitation ratio is defined as the digitated length over the boundary length. The process length ($\mu$m) is the average length of the measured processes. The quantification method is described in Figure S7. Data were analyzed by one-way ANOVA. (K) The concentration of transferred albumin in the middle well for the hydrogel tube (Tube), hydrogel tube with knot (Knot (-topo)), and hydrogel tube with knot and microconvex topography (Knot (+topo)) with cells being differentiated for 0, 6, 10, and 14 days was tested. The concentration was normalized to the concentration of transferred albumin measured for the cell-free scaffold on day 0. The normalized concentrations of each group were analyzed by one-way repeated measures ANOVA over time. The normalized concentrations of the three groups on Day 0, Day 6, Day 10, and Day 14 were analyzed by one-way ANOVA. Data are shown as average ± s.d., * $p < 0.05$, ** $p < 0.01$.

binding of antibodies onto the 3D cell layer might cause the inhomogeneous signal distribution. Moreover, we acquired the fluoresce image from different layers by using confocal microscopy and then did z-stacking to get the fluorescence image of the whole knot. Because the liquid and the hydrogel would cause light scattering and affect the signal, the fluorescence signals from different layers naturally vary. The above problems made it difficult to compare the intensity of the signal from the 3D cell layer. Thus, we did not use the fluorescence intensity of the immunostaining images to make a comparison for the following experiments.

Due to the perfusable bioreactor, the permeability test can be used to test the cell barrier function. The development of podocyte barrier function during differentiation (Diff) was tracked by the permeability test and compared with the nondifferentiated group (Ctr) (Figure 4I). The cell density of the two groups on day 14 showed no significant difference (Figure 4J). However, the transferred albumin decreased significantly over time for the "Diff" group but not for the "Ctr" group (Figure 4K), suggesting that podocyte differentiation was important for the development of barrier function over time.

To demonstrate the effect of microtopography, we compared the arrangement of actin fibers, together with the podocyte morphology, on the normal flat PDMS surface, hydrogel tube, and the hydrogel knot with and without microtopography (Figure 5A–J). *In vivo*, most of the glomerular F-actin is concentrated in the foot processes, which envelop the looping capillaries and interdigitate with neighboring podocytes via slit diaphragms.[45] Cytoskeletal changes in podocytes are related to foot process effacement and impaired glomerular filtration.[46] More branched and interdigitated actin fibers were found on the knot with microconvex topography (Figure 5A–D). These interdigitated


https://dx.doi.org/10.1021/acscentsci.9b01097
ACS Cent. Sci. XXXX, XXX, XXX–XXX

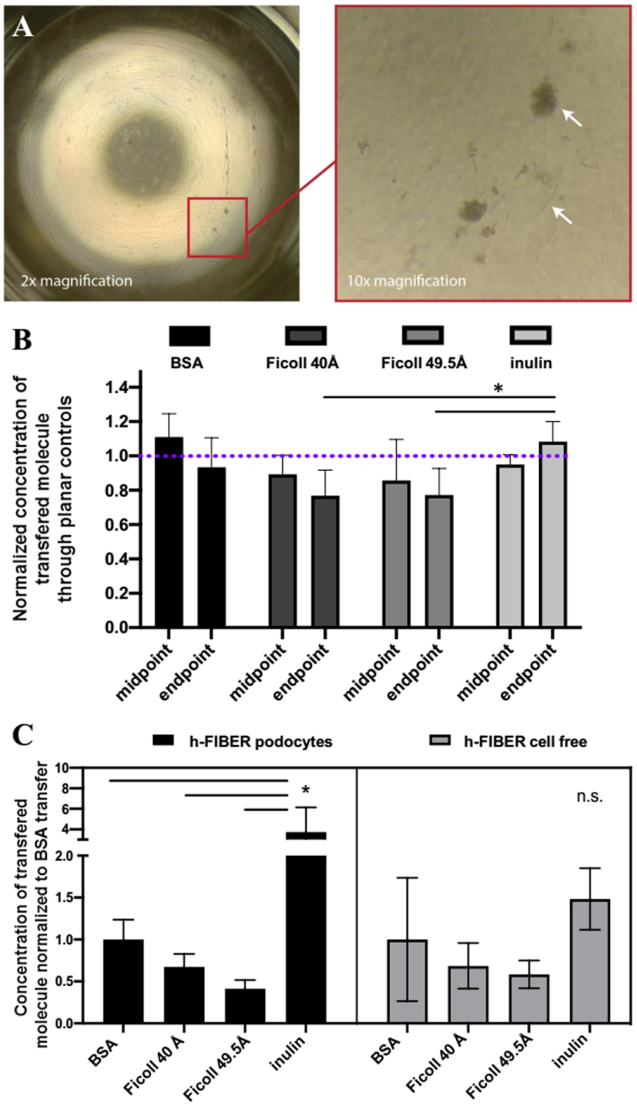


**Figure 6.** The 3D topography of h-FIBER contributes to a biomimetic size-discriminant barrier function. (A) Podocytes on planar alginate. (B) Permeability on planar controls. Permeability results for various FITC-labeled molecules across podocytes grown on planar alginate membranes, normalized to cell-free controls. Midpoint measurements were taken between days 6 and 9; endpoint measurements were taken between days 13 and 16. $n$ = 5 samples with cells were normalized to the average of $n$ = 4 cell-free samples. Repeated measures 2-way ANOVA confirms no significant difference over time between molecule transfer at midpoint and endpoint of differentiation time. At the endpoint, inulin had significantly more molecule transfer than Ficoll-40 (Ficoll 40 Å) and Ficoll-70 (Ficoll 49.5 Å), $p < 0.05$, but there was no significant difference between BSA and inulin. (C) Concentration of FITC-labeled BSA, inulin, Ficoll 40 Å, and Ficoll 49.5 Å, that was transferred across h-FIBERs with fixed podocytes or cell-free h-FIBERs, normalized to average BSA transfer, respectively. ANOVA confirms molecular-weight-dependent barrier function in configuration with fixed cells, whereas there was no significant difference in cell-free h-FIBERs. * $p < 0.05$.

actin fibers are most likely used by the podocytes to remain positioned on the soft curved surface similar to the surface provided by the looping capillaries. *In vivo*, podocytes are exposed to tremendous physical forces, requiring concentrated F-actin to provide mechanical support and efficient attachment.[47] Similar cytoskeletal structure is reported to be induced by stretch,[21,48] flow stimulation,[49] and topographic stimulation.[27]

The podocytes' morphologies on the flat substrate, tube, and knot with/without microtopographies were also analyzed by SEM (Figure 5E–H). On the tube region, podocytes tended to elongate and align along the long axis of the tube (Figure 5F). Podocytes cultivated on the flat substrate (Figure 5E) and the knot without microtopography (Figure 5G) were more spread out compared to those on the tube but did not develop an appreciable *in vivo*-like arborized morphology. On the hydrogel knot with microtopography, podocytes exhibited more and longer *in vivo*-like branched interdigitations (Figure 5H). To confirm the morphology differences, we quantified the digitation ratio and the average process length of podocytes cultivated on the different substrates (Figure 5I,J) according to the previously published method.[27] The digitation ratio and process length of podocytes on the knot with microtopography are greater than that of podocytes on the knot without microtopography and are significantly greater than that of podocytes on the tube, suggesting that the microconvex topography improves the digitation and extension of processes in podocytes. Collectively, these data indicate that the knot region with microtopography is essential for providing the *in vivo*-like microenvironment for podocytes.

The development of podocyte barrier function during differentiation on the tube (Tube), the knotted tube (Knot (-topo)), and the knotted tube with microtopography (Knot (+topo)) was tracked by the permeability test (Figure 5K). One-way repeated measures ANOVA showed that the transferred BSA decreased significantly over time for the "Knot (-topo)" group and the "Knot (+topo)" group, but not for the "Tube" group. Thus, the knot region is important for the development of podocyte barrier function. On day 14, the transfer of albumin from the lumen to the middle well for the "Knot (-topo)" group was significantly higher than that for the "Knot (+topo)" group, indicating that the microtopography is important for maintaining the *in vivo*-like cell function. Thus, the "concave and convex" geometries facilitated the formation of podocytes' actin fibers, arborized morphology, as well as the establishment of higher barrier function.

To observe differences in transport properties as a result of molecule type, Ficoll-70 (70 kDa, ~49.5 Å) and Ficoll-40 (40 kDa, ~40 Å) permeability across the podocyte barrier was tested alongside both BSA and inulin (5.5 kDa). A planar transwell insert with a layer of RGD-alginate was used as a control. It was observed that cells on planar controls grew poorly, with a tendency to detach from the surface or become elongated in morphology (Figure 6A). We suspect that, in the h-FIBER configuration, the factors of curvature, microtopography, and flow all contributed to allowing cells to grow and develop with higher success rates than on planar 2D alginate surfaces. Permeability tests also demonstrated that the cells grown on planar alginate surfaces did not contribute significantly to barrier function compared to cell-free controls, and barrier function did not improve significantly with the differentiation time, as transfer levels remained nearly equivalent (1.0) when normalized to cell-free controls (Figure 6B). This is different from h-FIBER permeability results, where differentiated cells reduced transfer of BSA to below 0.2 (Figure 5K). Moreover, inulin was nearly 4 times more permeable across the h-FIBER with the podocyte layer than BSA, whereas Ficoll 49.5 Å and Ficoll 40 Å were less permeable than BSA, with Ficoll 40 Å having the most similar


https://dx.doi.org/10.1021/acscentsci.9b01097
ACS Cent. Sci. XXXX, XXX, XXX−XXX

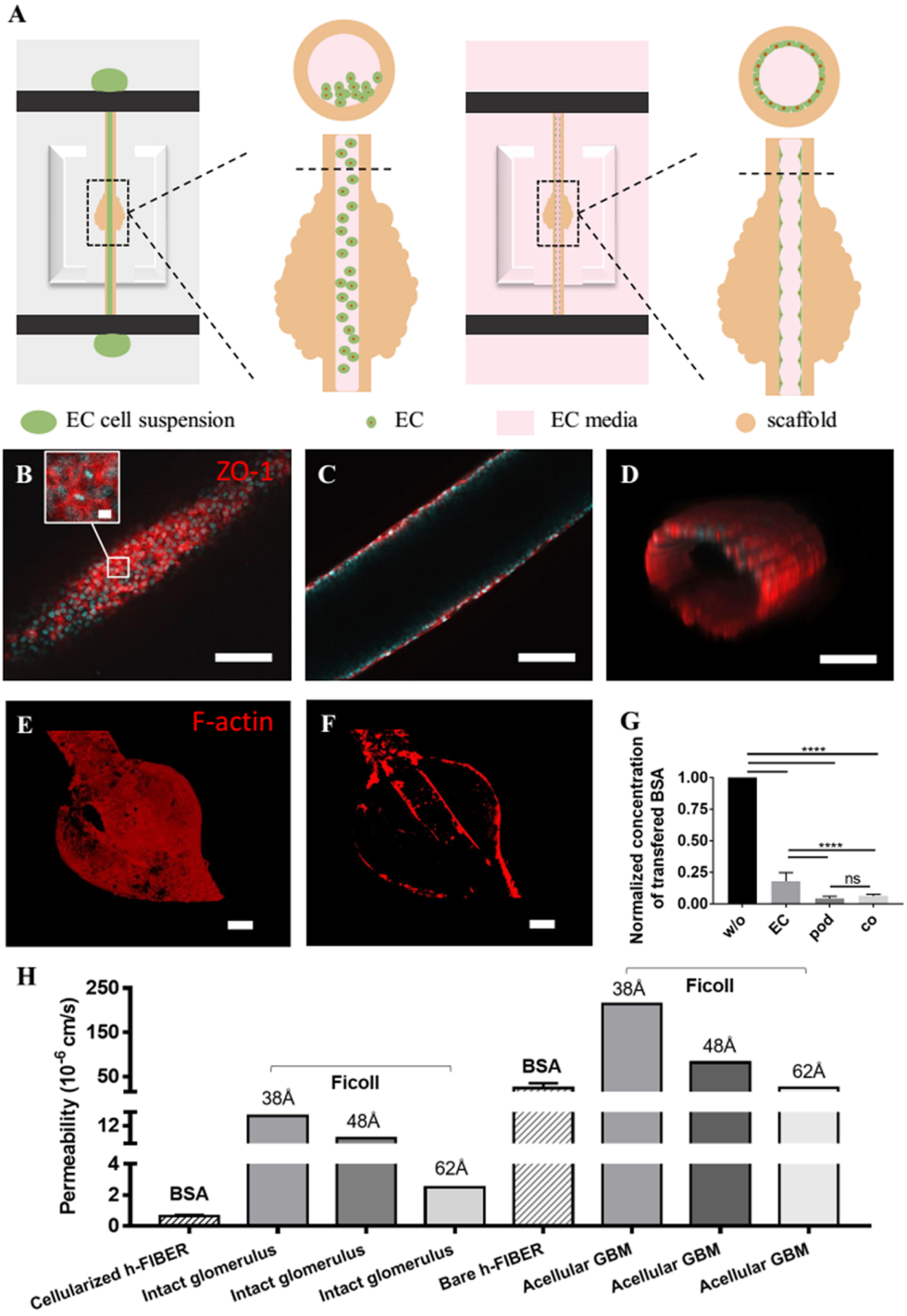


**Figure 7.** Endothelialization and the formation of the glomerular filtration barrier. (A) Illustration of cell seeding in the lumen of h-FIBER. (B–D) Confocal microscopy images showing ZO-1 (red) and DAPI (blue) staining of EC barrier formed in the lumen. Part B shows the bottom plane with inset showing the enlarged view. Part C shows the middle plane. Part D shows the 3D view of the EC barrier. (E) Front view of the glomerular structure stained for F-actin. (F) Longitudinal cross-sectional view of the glomerular structure formed on the h-FIBER with EC layer in the lumen and podocyte layer on the external surface both stained for F-actin. (G) Normalized concentration of transferred BSA through the h-FIBERs without cells (w/o) (tested on day 0), with EC barrier (EC) (tested on day 8 after EC seeding), with podocyte barrier (pod) (tested on day 14 after podocyte differentiation), and with both EC and podocyte barrier (co) (tested on day 8 after EC seeding). (H) Comparison of the permeability of the h-FIBER and glomerulus. Though the radius of BSA is around 36 Å, the fractional clearance of albumin was reported to be similar to the fractional clearances of Ficoll with Stokes–Einstein radius of 54 Å.[60] Thus, the permeability of Ficoll of similar sizes (38, 48, and 62 Å) from the intact glomerulus and acellular GBM tested *in vitro* were chosen as comparisons.[61] Data were analyzed by one-way ANOVA and are shown as average ± s.d., **** $p < 0.0001$. The scale bar in the inset of part B is 20 $\mu$m. The other scale bars are 100 $\mu$m.

(~70%) permeability values to BSA (Figure 6C). While the fixed podocyte h-FIBERs had a size-discriminating effect on the concentration of transferred molecules, the cell-free h-FIBERs did not significantly or preferentially influence the


https://dx.doi.org/10.1021/acscentsci.9b01097
ACS Cent. Sci. XXXX, XXX, XXX–XXX

transport properties of the molecules (Figure 6C). Overall, these data confirm the contribution of 3D cell barrier function to size discrimination.

Doxorubicin, widely used in antitumor therapy, is known to cause podocyte injury and induce proteinuria.[50,51] To model the intravenous injection of doxorubicin, we added culture medium with 1 $\mu$g mL$^{-1}$ doxorubicin into the inlet and outlet. BSA transferring through the drug-treated podocyte barrier increased in comparison to the control group (Figure S8), however, with milder cell barrier injury than previously reported.[16,21] The slope of permeability changes over time shows a significant difference between the drug-treated group and control group (Figure S8B), suggesting that the changes might be more significant if the drug exposure time is extended. These results demonstrated the potential application of the 3D glomerulus model in building a nephropathy model *in vitro*. This milder cell barrier injury might be because the drug in our model was perfused in the lumen, and thus, the podocytes on the outer surface of the h-FIBER scaffold were not directly exposed to the drug in high concentration. Another possible reason is that greater maturation in 3D tissues makes it more difficult for a drug to saturate a tissue and fulfill its targeted effect and thus contributes to greater robustness and resistance to drugs, which was also demonstrated in other 3D models previously.[52] The value of organ-on-a-chip systems is in reducing both false positives and false negatives in preclinical drug discovery and testing of new chemical entities. With a view of eliminating false positives, this feature may be desirable. We will explore the application of the platform in drug screening with more experiments in the future. Overall, with the current system and results, we can define specific advantages of our platform in drug testing. For example, our platform allows robust permeability tests by facile fluid sampling from the open-access wells, which will be suitable for regular workflow in the pharmaceutical industry.

At the blood vessel side *in vivo*, there is a layer of ECs in the capillary lumen, which is an important component of the functional filtration barrier.[23] The perfusable lumen in the h-FIBER is ideal for mimicking vascular lumen. Since the h-FIBER has been robustly assembled in the 96-well bioreactor, the seeding of ECs in the microscale hydrogel lumen was easily realized using the standard pipetting technique (Figure 7A). As the ECs proliferated and spread, a confluent EC layer covering the luminal surface was formed as confirmed with staining for ZO-1 (Figure 7B–D), a tight junction protein, as well as VE-Cadherin, an endothelial cell-specific protein (Figure S9). Compared to the cell-free h-FIBER, the permeability of the h-FIBER with ECs reduced significantly (Figure 7G), which further demonstrated the formation of a functional vascular barrier.

By culturing podocytes on the external surface and ECs on the lumen surface, a 3D glomerular filtration barrier was formed on the h-FIBER. The established glomerulus-like structure was demonstrated by F-actin staining (Figure 7E,F), demonstrating two cell layers in a precise geometrical arrangement. The permeability of the h-FIBER with both podocyte and EC layers was reduced significantly when compared to the h-FIBER with the EC layer only but did not show a significant difference when compared to the h-FIBER with the podocyte layer alone (Figure 6G). This result suggests that, in our glomerulus model, the podocyte layer contributed more to the barrier function, which is consistent with *in vivo* data showing that podocyte injury is a pivotal event resulting in proteinuria.[53] Moreover, the permeability of the h-FIBER was estimated according to the method and the mathematical model described in the experimental section. The results are shown in Figure 7H, suggesting that the h-FIBER is slightly less permeable than acellular glomerulus basement membrane (GBM), and the cellularized h-FIBER is also slightly less permeable than the intact glomerulus. Though the physical separation of the two cell types in our model is much greater than *in vivo* (0.3 $\mu$m), and the cells were from nonhuman cell sources, limiting utility of this work in modeling a human system with proper cell–cell crosstalk, these results demonstrate the potential and the feasibility of this platform. In future work, we plan to use human cells (e.g., podocytes from human induced pluripotent stem cells[21]) and try to minimize the thickness of the alginate layer to further develop a more physiological model.

The generation of shape-controlled hydrogel scaffolds using microfluidics has drawn considerable attention for its ability to mimic different tissue constructs.[54] Through precise control of fluids in the microdevices, various hollow microfibers with straight,[55] folded,[56] helical,[57] and multiple channels[58] have been mass-produced to mimic complex vascular microenvironments. However, achieving a perfusable vascular barrier within these microscaffolds was still a challenge. This limitation was rooted in the lack of a suitable bioreactor to provide reliable perfusion and the difficulty in seeding and culturing cells inside the fragile microscale hydrogel scaffolds. Here, we described a 96-well plate platform based on the h-FIBER that overcame these limitations and provided a functional glomerulus-on-a-plate.

## 3. CONCLUSIONS

In summary, a novel perfusable 3D engineered glomerulus based on a microfluidic extruded topographic hydrogel scaffold has been demonstrated here. The h-FIBERs were produced by microfluidic spinning technology with a chemically induced inflation method, developed to fabricate microconvex topographies on the 3D hydrogel surface for mimicking microcurved features of the looping capillaries. The assembly of the h-FIBERs into a 96-well plate allowed perfusion, cell maintenance, and a permeability test to be realized using a standard pipetting technique. Endothelial cells were seeded in the perfusable lumen to generate the vascular barrier. The podocyte layer with better barrier function was formed on capillary loop-like structures. The permeability of albumin from the vascular channel to the ultrafiltrate side was tested, demonstrating the successful fabrication of a 3D glomerulus filtration barrier. The combination of the newly developed h-FIBERs using microfluidics and coculture in a 96-well plate setting to control cell arrangement demonstrates a new approach to assemble a biomimetic glomerulus in 3D.

## ■ ASSOCIATED CONTENT

### Supporting Information

The Supporting Information is available free of charge at https://pubs.acs.org/doi/10.1021/acscentsci.9b01097.

Additional experimental details and figures including schematics, knot sizes, viability test results, SEM images, permeability test results, confocal microscopy images, and diffusion coefficients (PDF)

Video S1: fluorescent beads perfused through the h-FIBER lumen driven by hydrostatic pressure (MP4)



https://dx.doi.org/10.1021/acscentsci.9b01097
ACS Cent. Sci. XXXX, XXX, XXX−XXX

## AUTHOR INFORMATION


### Corresponding Authors

**Qionglin Liang** − *MOE Key Laboratory of Bioorganic Phosphorus Chemistry & Chemical Biology, Beijing Key Lab of Microanalytical Methods & Instrumentation, Department of Chemistry, Centre for Synthetic and Systems Biology, Tsinghua University, Beijing 100084, P. R. China;* orcid.org/0000-0002-6750-038X; Email: liangql@tsinghua.edu.cn

**Milica Radisic** − *Institute for Biomaterials and Biomedical Engineering and Department of Chemical Engineering and Applied Chemistry, University of Toronto, Toronto, Ontario M5S 3G9, Canada;* orcid.org/0000-0003-1249-4135; Email: m.radisic@utoronto.ca

### Authors

**Ruoxiao Xie** − *MOE Key Laboratory of Bioorganic Phosphorus Chemistry & Chemical Biology, Beijing Key Lab of Microanalytical Methods & Instrumentation, Department of Chemistry, Centre for Synthetic and Systems Biology, Tsinghua University, Beijing 100084, P. R. China; Institute for Biomaterials and Biomedical Engineering, University of Toronto, Toronto, Ontario M5S 3G9, Canada*

**Anastasia Korolj** − *Institute for Biomaterials and Biomedical Engineering and Department of Chemical Engineering and Applied Chemistry, University of Toronto, Toronto, Ontario M5S 3G9, Canada;* orcid.org/0000-0002-1872-3923

**Chuan Liu** − *Institute for Biomaterials and Biomedical Engineering, University of Toronto, Toronto, Ontario M5S 3G9, Canada*

**Xin Song** − *Department of Chemical Engineering and Applied Chemistry, University of Toronto, Toronto, Ontario M5T 3A1, Canada*

**Rick Xing Ze Lu** − *Institute for Biomaterials and Biomedical Engineering, University of Toronto, Toronto, Ontario M5S 3G9, Canada*

**Boyang Zhang** − *Institute for Biomaterials and Biomedical Engineering, University of Toronto, Toronto, Ontario M5S 3G9, Canada*

**Arun Ramachandran** − *Department of Chemical Engineering and Applied Chemistry, University of Toronto, Toronto, Ontario M5T 3A1, Canada;* orcid.org/0000-0001-9403-5930

Complete contact information is available at: https://pubs.acs.org/10.1021/acscentsci.9b01097


### Notes

The authors declare no competing financial interest.

## ACKNOWLEDGMENTS

This work was made possible by the Natural Sciences and Engineering Research Council of Canada (NSERC) Collaborative Research and Development Grant (CRDPJ 5011), China Scholarship Council (201706210353) to R.X., NSERC Alexander Graham Bell Canada Graduate Scholarships to A.K., and the CIHR Banting Postdoctoral Fellowship to B.Z. This work was also funded by the National Natural Science Foundation of China (81872835), Ministry of Science and Technology of China (2017YFC0906902 and 2017ZX09301032), Canadian Institutes of Health Research (CIHR) Operating Grants (MOP-126027 and MOP-137107), and NSERC Discovery Grant (RGPIN 326982-10). The authors would like to thank Anrea Lam for illustration in Figure 1A.

## REFERENCES


(1) Siramshetty, V. B.; Nickel, J.; Omieczynski, C.; Gohlke, B.; Drwal, M. N.; Preissner, R. WITHDRAWN—a resource for withdrawn and discontinued drugs. *Nucleic Acids Res.* **2016**, *44*, D1080−D1086.

(2) Kim, S. Y.; Moon, A. Drug-induced nephrotoxicity and its biomarkers. *Biomol. Ther.* **2012**, *20*, 268.

(3) Shen, J. X.; Youhanna, S.; Zandi Shafagh, R.; Kele, J.; Lauschke, V. M. Organotypic and microphysiological models of liver, gut, and kidney for studies of drug metabolism, pharmacokinetics, and toxicity. *Chem. Res. Toxicol.* **2020**, *33*, 38−60.

(4) Al-Awqati, Q.; Oliver, J. A. Stem cells in the kidney. *Kidney Int.* **2002**, *61*, 387−395.

(5) Bryer, J. S.; Susztak, K. Screening drugs for kidney disease: targeting the podocyte. *Cell Chem. Biol.* **2018**, *25*, 126−127.

(6) Lih, E.; Park, W.; Park, K. W.; Chun, S. Y.; Kim, H.; Joung, Y. K.; Kwon, T. G.; Hubbell, J. A.; Han, D. K. A bioinspired scaffold with anti-inflammatory magnesium hydroxide and decellularized extracellular matrix for renal tissue regeneration. *ACS Cent. Sci.* **2019**, *5*, 458−467.

(7) Homan, K. A.; Gupta, N.; Kroll, K. T.; Kolesky, D. B.; Skylar-Scott, M.; Miyoshi, T.; Mau, D.; Valerius, M. T.; Ferrante, T.; Bonventre, J. V. Flow-enhanced vascularization and maturation of kidney organoids in vitro. *Nat. Methods* **2019**, *16*, 255−262.

(8) Freedman, B. S.; Brooks, C. R.; Lam, A. Q.; Fu, H.; Morizane, R.; Agrawal, V.; Saad, A. F.; Li, M. K.; Hughes, M. R.; Vander Werff, R. Modelling kidney disease with CRISPR-mutant kidney organoids derived from human pluripotent epiblast spheroids. *Nat. Commun.* **2015**, *6*, 8715.

(9) Takasato, M.; Pei, X. E.; Chiu, H. S.; Maier, B.; Baillie, G. J.; Ferguson, C.; Parton, R. G.; Wolvetang, E. J.; Roost, M. S.; de Sousa Lopes, S. M. C. Kidney organoids from human iPS cells contain multiple lineages and model human nephrogenesis. *Nature* **2015**, *526*, 564−568.

(10) Morizane, R.; Bonventre, J. V. Kidney organoids: a translational journey. *Trends Mol. Med.* **2017**, *23*, 246−263.

(11) Bantounas, I.; Ranjzad, P.; Tengku, F.; Silajdžić, E.; Forster, D.; Asselin, M.; Lewis, P.; Lennon, R.; Plagge, A.; Wang, Q. Generation of functioning nephrons by implanting human pluripotent stem cell-derived kidney progenitors. *Stem Cell Rep.* **2018**, *10*, 766−779.

(12) Li, M.; Corbelli, A.; Watanabe, S.; Armelloni, S.; Ikehata, M.; Parazzi, V.; Pignatari, C.; Giardino, L.; Mattinzoli, D.; Lazzari, L.; et al. Three-dimensional podocyte−endothelial cell co-cultures: Assembly, validation, and application to drug testing and intercellular signaling studies. *Eur. J. Pharm. Sci.* **2016**, *86*, 1−12.

(13) Colombo, C.; Li, M.; Watanabe, S.; Messa, P.; Edefonti, A.; Montini, G.; Moscatelli, D.; Rastaldi, M. P.; Cellesi, F. Polymer nanoparticle engineering for podocyte repair: from in vitro models to new nanotherapeutics in kidney diseases. *ACS Omega* **2017**, *2*, 599−610.

(14) Zhang, B.; Korolj, A.; Lai, B. F. L.; Radisic, M. Advances in organ-on-a-chip engineering. *Nat. Rev. Mater.* **2018**, *3*, 257−278.

(15) Wilmer, M. J.; Ng, C. P.; Lanz, H. L.; Vulto, P.; Suter-Dick, L.; Masereeuw, R. Kidney-on-a-Chip Technology for Drug-Induced Nephrotoxicity Screening. *Trends Biotechnol.* **2016**, *34*, 156−170.

(16) Qu, Y.; An, F.; Luo, Y.; Lu, Y.; Liu, T.; Zhao, W.; Lin, B. A nephron model for study of drug-induced acute kidney injury and assessment of drug-induced nephrotoxicity. *Biomaterials* **2018**, *155*, 41−53.

(17) Sakolish, C. M.; Mahler, G. J. A novel microfluidic device to model the human proximal tubule and glomerulus. *RSC Adv.* **2017**, *7*, 4216−4225.

(18) Petrosyan, A.; Cravedi, P.; Villani, V.; Angeletti, A.; Manrique, J.; Renieri, A.; De Filippo, R. E.; Perin, L.; Da Sacco, S. A glomerulus-on-a-chip to recapitulate the human glomerular filtration barrier. *Nat. Commun.* **2019**, *10*, 1−17.




https://dx.doi.org/10.1021/acscentsci.9b01097
ACS Cent. Sci. XXXX, XXX, XXX−XXX

(19) Wang, L.; Tao, T.; Su, W.; Yu, H.; Yu, Y.; Qin, J. A disease model of diabetic nephropathy in a glomerulus-on-a-chip microdevice. *Lab Chip* **2017**, *17*, 1749−1760.
(20) Zhou, M.; Zhang, X.; Wen, X.; Wu, T.; Wang, W.; Yang, M.; Wang, J.; Fang, M.; Lin, B.; Lin, H. Development of a functional glomerulus at the organ level on a chip to mimic hypertensive nephropathy. *Sci. Rep.* **2016**, *6*, 1−13.
(21) Musah, S.; Mammoto, A.; Ferrante, T. C.; Jeanty, S. S. F.; Hirano-Kobayashi, M.; Mammoto, T.; Roberts, K.; Chung, S.; Novak, R.; Ingram, M.; et al. Mature induced-pluripotent-stem-cell-derived human podocytes reconstitute kidney glomerular-capillary-wall function on a chip. *Nat. Biomed. Eng.* **2017**, *1*, 1−12.
(22) Du, B.; Yu, M.; Zheng, J. Transport and interactions of nanoparticles in the kidneys. *Nat. Rev. Mater.* **2018**, *3*, 358−374.
(23) Obeidat, M.; Obeidat, M.; Ballermann, B. J. Glomerular endothelium: A porous sieve and formidable barrier. *Exp. Cell Res.* **2012**, *318*, 964−972.
(24) Benam, K. H.; Dauth, S.; Hassell, B.; Herland, A.; Jain, A.; Jang, K.; Karalis, K.; Kim, H. J.; MacQueen, L.; Mahmoodian, R. Engineered in vitro disease models. *Annu. Rev. Pathol.: Mech. Dis.* **2015**, *10*, 195−262.
(25) Nichol, J. W.; Khademhosseini, A. Modular tissue engineering: engineering biological tissues from the bottom up. *Soft Matter* **2009**, *5*, 1312−1319.
(26) Khademhosseini, A.; Langer, R. Microengineered hydrogels for tissue engineering. *Biomaterials* **2007**, *28*, 5087−5092.
(27) Korolj, A.; Laschinger, C.; James, C.; Hu, E.; Velikonja, C.; Smith, N.; Gu, I.; Ahadian, S.; Willette, R.; Radisic, M. Curvature facilitates podocyte culture in a biomimetic platform. *Lab Chip* **2018**, *18*, 3112−3128.
(28) Lim, K. S.; Baptista, M.; Moon, S.; Woodfield, T. B.; Rnjak-Kovacina, J. Microchannels in development, survival, and vascularisation of tissue analogues for regenerative medicine. *Trends Biotechnol.* **2019**, *37*, 1189−1201.
(29) Xie, R.; Zheng, W.; Guan, L.; Ai, Y.; Liang, Q. Engineering of hydrogel materials with perfusable microchannels for building vascularized tissues. *Small* **2020**, *16*, 1902838.
(30) Polacheck, W. J.; Kutys, M. L.; Tefft, J. B.; Chen, C. S. Microfabricated blood vessels for modeling the vascular transport barrier. *Nat. Protoc.* **2019**, *14*, 1425−1454.
(31) Huber, D.; Oskooei, A.; Casadevall I Solvas, X.; Demello, A.; Kaigala, G. V. Hydrodynamics in cell studies. *Chem. Rev.* **2018**, *118*, 2042−2079.
(32) Kutys, M. L.; Chen, C. S. Forces and mechanotransduction in 3D vascular biology. *Curr. Opin. Cell Biol.* **2016**, *42*, 73−79.
(33) Xie, R.; Xu, P.; Liu, Y.; Li, L.; Luo, G.; Ding, M.; Liang, Q. Necklace-like microfibers with variable knots and perfusable channels fabricated by an oil-free microfluidic spinning process. *Adv. Mater.* **2018**, *30*, 1705082.
(34) Huebsch, N.; Arany, P. R.; Mao, A. S.; Shvartsman, D.; Ali, O. A.; Bencherif, S. A.; Rivera-Feliciano, J.; Mooney, D. J. Harnessing traction-mediated manipulation of the cell/matrix interface to control stem-cell fate. *Nat. Mater.* **2010**, *9*, 518−526.
(35) Chai, Y.; Mei, L. H.; Wu, G. L.; Lin, D. Q.; Yao, S. J. Gelation conditions and transport properties of hollow calcium alginate capsules. *Biotechnol. Bioeng.* **2004**, *87*, 228−233.
(36) Li, R. H.; Altreuter, D. H.; Gentile, F. T. Transport characterization of hydrogel matrices for cell encapsulation. *Biotechnol. Bioeng.* **1996**, *50*, 365−373.
(37) Axelsson, A.; Persson, B. Determination of effective diffusion coefficients in calcium alginate gel plates with varying yeast cell content. *Appl. Biochem. Biotechnol.* **1988**, *18*, 231−250.
(38) Tanaka, H.; Matsumura, M.; Veliky, I. A. Diffusion characteristics of substrates in Ca-alginate gel beads. *Biotechnol. Bioeng.* **1984**, *26*, 53−58.
(39) Lai, B. F. L.; Huyer, L. D.; Lu, R. X. Z.; Drecun, S.; Radisic, M.; Zhang, B. InVADE: Integrated vasculature for assessing dynamic events. *Adv. Funct. Mater.* **2017**, *27*, 1703524.
(40) Zhang, B.; Montgomery, M.; Chamberlain, M. D.; Ogawa, S.; Korolj, A.; Pahnke, A.; Wells, L. A.; Massé, S.; Kim, J.; Reis, L.; et al. Biodegradable scaffold with built-in vasculature for organ-on-a-chip engineering and direct surgical anastomosis. *Nat. Mater.* **2016**, *15*, 669−678.
(41) Zhang, B.; Lai, B. F. L.; Xie, R.; Huyer, L. D.; Montgomery, M.; Radisic, M. Microfabrication of AngioChip, a biodegradable polymer scaffold with microfluidic vasculature. *Nat. Protoc.* **2018**, *13*, 1793−1813.
(42) Ballermann, B. J.; Dardik, A.; Eng, E.; Liu, A. Shear stress and the endothelium. *Kidney Int.* **1998**, *54*, 100−108.
(43) Ruotsalainen, V.; Ljungberg, P.; Wartiovaara, J.; Lenkkeri, U.; Kestilä, M.; Jalanko, H.; Holmberg, C.; Tryggvason, K. Nephrin is specifically located at the slit diaphragm of glomerular podocytes. *Proc. Natl. Acad. Sci. U. S. A.* **1999**, *96*, 7962−7967.
(44) Shankland, S. J.; Pippin, J. W.; Reiser, J.; Mundel, P. Podocytes in culture: past, present, and future. *Kidney Int.* **2007**, *72*, 26−36.
(45) Andrews, P. M.; Bates, S. B. Filamentous actin bundles in the kidney. *Anat. Rec.* **1984**, *210*, 1−9.
(46) Perico, L.; Conti, S.; Benigni, A.; Remuzzi, G. Podocyte−actin dynamics in health and disease. *Nat. Rev. Nephrol.* **2016**, *12*, 692.
(47) Schell, C.; Huber, T. B. The evolving complexity of the podocyte cytoskeleton. *J. Am. Soc. Nephrol.* **2017**, *28*, 3166−3174.
(48) Endlich, N.; Kress, K. R.; Reiser, J.; Uttenweiler, D.; Kriz, W.; Mundel, P.; Endlich, K. Podocytes respond to mechanical stress in vitro. *J. Am. Soc. Nephrol.* **2001**, *12*, 413−422.
(49) Friedrich, C.; Endlich, N.; Kriz, W.; Endlich, K. Podocytes are sensitive to fluid shear stress in vitro. *Am. J. Physiol.* **2006**, *291*, F856−F865.
(50) Zhang, H.; Wang, W.; Ren, L.; Zhao, X.; Wang, Z.; Zhuang, D.; Bai, Y. The mTORC2/Akt/NFκB pathway-mediated activation of TRPC6 participates in adriamycin-induced podocyte apoptosis. *Cell. Physiol. Biochem.* **2016**, *40*, 1079−1093.
(51) Lee, J.; Kim, S. Kidney-on-a-chip: a new technology for predicting drug efficacy, interactions, and drug-induced nephrotoxicity. *Curr. Drug Metab.* **2018**, *19*, 577−583.
(52) Breslin, S.; O'Driscoll, L. The relevance of using 3D cell cultures, in addition to 2D monolayer cultures, when evaluating breast cancer drug sensitivity and resistance. *Oncotarget* **2016**, *7*, 45745.
(53) Brinkkoetter, P. T.; Ising, C.; Benzing, T. The role of the podocyte in albumin filtration. *Nat. Rev. Nephrol.* **2013**, *9*, 328−336.
(54) Ma, S.; Mukherjee, N. Microfluidics fabrication of soft microtissues and bottom-up assembly. *Adv. Biosyst.* **2018**, *2*, 1800119.
(55) Pi, Q.; Maharjan, S.; Yan, X.; Liu, X.; Singh, B.; van Genderen, A. M.; Robledo-Padilla, F.; Parra-Saldivar, R.; Hu, N.; Jia, W.; et al. Digitally tunable microfluidic bioprinting of multilayered cannular tissues. *Adv. Mater.* **2018**, *30*, 1706913.
(56) Liu, Y.; Xu, P.; Liang, Z.; Xie, R.; Ding, M.; Liu, H.; Liang, Q. Hydrogel microfibers with perfusable folded channels for tissue constructs with folded morphology. *RSC Adv.* **2018**, *8*, 23475−23480.
(57) Xu, P.; Xie, R.; Liu, Y.; Luo, G.; Ding, M.; Liang, Q. Bioinspired microfibers with embedded perfusable helical channels. *Adv. Mater.* **2017**, *29*, 1701664.
(58) Cheng, Y.; Zheng, F.; Lu, J.; Shang, L.; Xie, Z.; Zhao, Y.; Chen, Y.; Gu, Z. Bioinspired multicompartmental microfibers from microfluidics. *Adv. Mater.* **2014**, *26*, 5184−5190.
(59) Puelles, V. G.; Douglas-Denton, R. N.; Cullen-McEwen, L. A.; Li, J.; Hughson, M. D.; Hoy, W. E.; Kerr, P. G.; Bertram, J. F. Podocyte number in children and adults: associations with glomerular size and numbers of other glomerular resident cells. *J. Am. Soc. Nephrol.* **2015**, *26*, 2277−2288.
(60) Ohlson, M.; Sörensson, J.; Haraldsson, B. Glomerular size and charge selectivity in the rat as revealed by FITC-Ficoll and albumin. *Am. J. Physiol.* **2000**, *279*, 84−91.
(61) Edwards, A.; Deen, W. M.; Daniels, B. S. Hindered transport of macromolecules in isolated glomeruli. I. Diffusion across intact and cell-free capillaries. *Biophys. J.* **1997**, *72*, 204−213.


https://dx.doi.org/10.1021/acscentsci.9b01097
ACS Cent. Sci. XXXX, XXX, XXX−XXX